

Lyapunov instabilities of Lennard-Jones fluids

Hong-liu Yang* and Günter Radons†

Institute of Physics

Chemnitz University of Technology,

D-09107 Chemnitz, Germany

(Dated: November 11, 2018)

Recent work on many particle system reveals the existence of regular collective perturbations corresponding to the smallest positive Lyapunov exponents (LEs), called hydrodynamic Lyapunov modes. Until now, however, these modes are only found for hard core systems. Here we report new results on Lyapunov spectra and Lyapunov vectors (LVs) for Lennard-Jones fluids. By considering the Fourier transform of the coordinate fluctuation density $u^{(\alpha)}(x, t)$, it is found that the LVs with $\lambda \approx 0$ are highly dominated by a few components with low wave-numbers. These numerical results provide strong evidence that hydrodynamic Lyapunov modes do exist in soft-potential systems, although the collective Lyapunov modes are more vague than in hard-core systems. In studying the density and temperature dependence of these modes, it is found that, when the value of Lyapunov exponent $\lambda^{(\alpha)}$ is plotted as function of the dominant wave number k_{max} of the corresponding LV, all data from simulations with different densities and temperatures collapse onto a single curve. This shows that the dispersion relation $\lambda^{(\alpha)}$ vs. k_{max} for hydrodynamical Lyapunov modes appears to be universal irrespective of the particle density and temperature of the system. Despite the wave-like character of the LVs, no step-like structure exists in the Lyapunov spectrum of the systems studied here, in contrast to the hard-core case. Further numerical simulations show that the finite-time LEs fluctuate strongly. We have also investigated localization features of LVs and propose a new length scale to characterize the Hamiltonian spatio-temporal chaotic states.

PACS numbers: 05.45.-a, 05.20.-y, 02.70.Ns, 05.20.Jn, 05.45.Jj

I. INTRODUCTION

One of the most successful theories in modern science is statistical mechanics, which allows one to understand the macroscopic (thermodynamic) properties of matter from a statistical analysis of the microscopic (mechanical) behavior of the constituent particles. In spite of this, using certain probabilistic assumptions such as Boltzmann's *Stosszahlansatz* renders the lack of a firm foundation of this theory, especially for non-equilibrium statistical mechanics. Fortunately, the concept of chaotic dynamics developed in the 20th century [1] is a good candidate for complying with these difficulties. Instead of the probabilistic assumptions, the dynamical instability of trajectories can provide the necessary fast loss of time correlations, ergodicity, mixing and other dynamical randomness [2]. It is generally expected that dynamical instability is at the origin of macroscopic transport phenomena and that one can find certain connection between them. In the past decade, some beautiful theories in this direction were already developed. Examples are the escape-rate formalism by Gaspard and Nicolis [3, 4] and the Gaussian thermostat method due to Nosé, Hoover, Evans, Morriss and others [5, 6, 7], where the Lyapunov exponents were related to certain transport coefficients.

Very recently, molecular dynamics simulations on hard-core systems revealed the existence of regular col-

lective perturbations corresponding to the smallest positive Lyapunov exponents (LEs), named hydrodynamic Lyapunov modes [8]. This opens a possible new way for the connection between Lyapunov vectors, a quantity characterizing dynamical instability of trajectories, and macroscopic transport properties. A lot of work [9, 10, 11, 12, 13, 14, 15, 16] has been done to identify this phenomenon and to find out its origin. It is commonly thought that the appearance of these modes is due to the conservation of certain quantities in the systems studied [10, 11, 12, 13, 14]. A natural consequence of this expectation is that the appearance of such modes would not be an exclusive feature of hard-core systems and should be generic to a large class of Hamiltonian systems. However, till now, these modes were only identified in the computer simulations of hard-core systems [9, 10, 16].

In this work, we report on new results about a 1d system with Lennard-Jones interaction. Although the identification of regular hydrodynamic Lyapunov modes by naked eye is difficult for soft potential systems [16], our new technique based on a spectral analysis of LVs shows strong evidence that hydrodynamic Lyapunov modes do exist in this case. The influence of density and temperature changes is studied in detail. The dispersion relation for hydrodynamic Lyapunov modes, the dominant wave-number as function of the corresponding LEs is found being universal for all densities and temperatures.

Furthermore we study the localization properties of LVs. Based on the extensive nature of LVs with $\lambda \approx 0$, we propose a new length scale to characterize a spatio-temporal chaotic Hamiltonian system. It is expected that this new quantity will be useful for the task of dis-

*Electronic address: hongliu.yang@physik.tu-chemnitz.de

†Electronic address: radons@physik.tu-chemnitz.de

tinguishing different spatio-temporal chaotic states and characterizing transitions among them. This is an important open question in the study of spatial-temporal chaos [17].

II. MODEL

In this study we use a 1D Lennard-Jones system with Hamiltonian

$$H = \sum_{i=1}^N mv_i^2/2 + \sum_{i<j} V(x_j - x_i) \quad (1)$$

The interaction potential among particles is of the form:

$$V(r) = \begin{cases} 4\epsilon [(\sigma/r)^{12} - (\sigma/r)^6] - V_c & \text{if } r \leq r_c, \\ 0 & \text{otherwise.} \end{cases} \quad (2)$$

with $V_c = 4\epsilon [(\sigma/r_c)^{12} - (\sigma/r_c)^6]$. The potential is truncated in order to lower the computational burden. Other types of potential with smoothed force at the truncation point were also simulated to check the influence on the results given below. No qualitative difference is found between them.

The system is integrated using the velocity form of the Verlet algorithm with periodic boundary conditions [18]. In our simulations, we set $m = 1$, $\sigma = 1$, $\epsilon = 1$ and $r_c = 2.5$. All results are given in reduced units, i.e., length in units of σ , energy in units of ϵ and time in units of $(m\sigma^2/48\epsilon)^{1/2}$. The time step used in the molecular dynamics simulation is $h = 0.008$. The standard Gram-Schmidt re-orthonormalization algorithm [19, 20] is used to calculate the local dynamical instability of the systems studied. The time interval for periodic re-orthonormalization is $30h$ to $100h$. Throughout this paper, the particle number typically is denoted by N , the length of the system by L and the temperature by T .

III. NUMERICAL RESULTS

A. The stationary state

In the numerical calculation of the Lyapunov instability of a many-body system [21], there are some important time scales to be kept in mind: the first one is the time for a many-body system to relax to a stationary state, which guarantees that quantities measured afterwards are not for a transient state; the second is the time for the set of Lyapunov vectors to relax to their right orientations since offset vectors are usually selected randomly at the beginning; the third is the time used to count LEs and LVs, which should be long enough to ensure that the trajectory wanders all over the attractor. For a many-body system like the one studied here, these time scales can

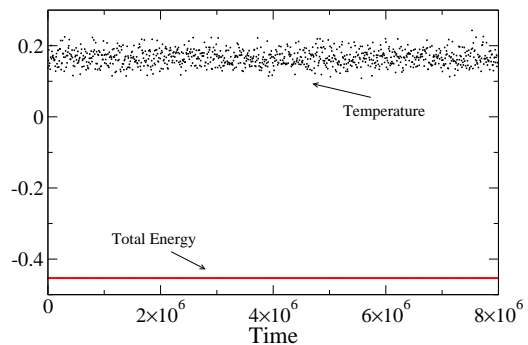


FIG. 1: Time evolution of temperature $T \equiv \langle mv^2 \rangle$ and total energy. The nearly constant state variables show that the system has reached already a stationary state. The parameter setting used here is: $N = 100$, $L = 1000$ and $T = 0.2$.

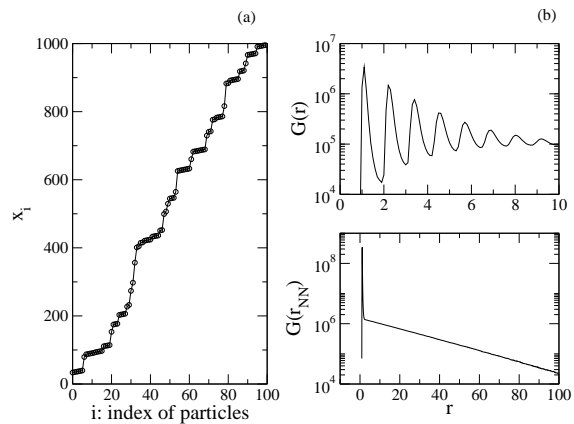


FIG. 2: a) Particle positions x_i vs. index of particles i and b) pair distribution function $G(r)$ for the space among all particles (upper panel) and nearest neighbors (lower panel) for the stationary state shown in Fig. 1 (see [24] for the definition of $G(r)$). The sharp peaks in $G(r)$ imply that the state is a broken-chain one.

be extremely long due to the large number of degrees of freedom involved [22, 23].

The time evolution of state variables like temperature T and total energy for a case with parameter setting $N = 100$, $L = 1000$ and $T = 0.2$ is shown in Fig. 1. In the beginning of our molecular dynamics simulation, particles are placed randomly in the interval $[0, L]$. Their velocities are chosen randomly from a Boltzmann distribution. In order to equilibrate the system, it is coupled to a stochastic heat bath with given temperature T , i.e., every 500 steps the velocities of the particles are replaced with velocities that were drawn from a Boltzmann distribution corresponding to that temperature. This was done for a time period of length t_{eq} , which is longer than the relaxation time of the system at this temperature. After the equilibration procedure, the system is allowed to evolve with constant total energy, i.e., without the heat bath, for a time period of the same length as t_{eq} , in order to be sure that the system is already in a stationary

state at given temperature T . In Fig. 1, the period with thermal bath is omitted and only the part of evolution with constant total energy is shown. The nearly constant value of temperature means that the system has already reached a stationary state and one can start the calculation of the Lyapunov instability of the system. The pair distribution function $G(r)$ shown in Fig. 2 tells us that the stationary state for $T = 0.2$ is a broken-chain state with short range order. This is generic for a 1d Lennard-Jones system with not too high density [25].

B. Benettin method using Gram-Schmidt orthogonalization

The standard method invented by Benettin and Shimada [19, 20] is the most efficient one to calculate the Lyapunov exponents and Lyapunov vectors of large systems. Here $N \times N$ linearized equations for offset vectors in the tangent space were integrated simultaneously with the set of N nonlinear equations for the reference trajectory. Offset vectors were periodically re-orthonormalized using the Gram-Schmidt algorithm. The resulting rescaling factors measure the expansion or contraction rate of offset vectors in certain directions. Averaging the logarithm of them for a period τ gets what are called *finite-time Lyapunov exponents* λ_τ . The limit $\lambda \equiv \lambda_{\tau \rightarrow +\infty}$ is what is usually called *Lyapunov exponent*. The value of finite-time LEs λ_τ depends on the trajectory segment where it is calculated and usually it fluctuates as the segment moves along the trajectory. However $\lambda_{+\infty}$ is time independent and unique for an ergodic system. In this sense, $\lambda_{+\infty}$ is a global quantity in characterizing the system attractor while the finite-time LEs are local quantities which contain more detailed information about the dynamics. The offset vectors just after re-orthonormalization are called *Lyapunov vectors*. It is a local quantity in characterizing the system attractor similar to the finite-time LEs.

Another point to be noted is that Lyapunov vectors obtained using Benettin's method are always mutually orthogonal while the local unstable and stable directions are in general not orthogonal. In this sense, these are two different sets of vectors. They are also different from the one in the multiplicative ergodic theorem [26]. Lyapunov vectors obtained in the standard way can at least represent the most unstable direction in a certain subspace and they already contain a lot of important information about the dynamical instability in tangent space. We will rely on them to continue our study in this paper.

C. Lyapunov exponents with wild fluctuations

The Lyapunov spectrum for the case with $N = 100$, $L = 1000$ and $T = 0.2$ is shown in Fig. 3. Here only half of the spectrum is shown since all LEs of Hamiltonian systems come in pairs according to the conjugate-pairing

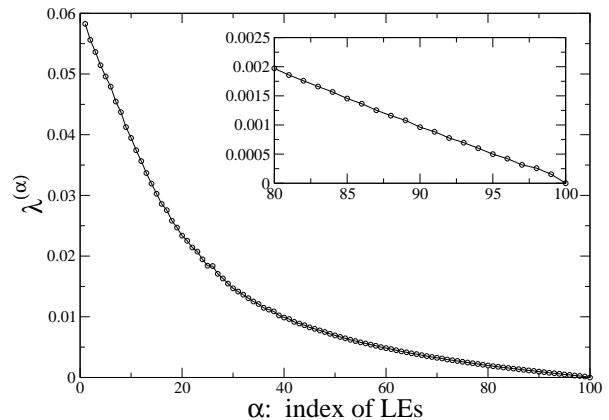


FIG. 3: Lyapunov spectrum for the state shown in Fig. 2. Enlargement of the part in the regime $\lambda^{(\alpha)} \approx 0$ is shown in the inset. It is the result of an average over 58 samples with different initial conditions and for each sample the averaging period is $4 \times 10^6 h$. Here no step-wise structure exists in contrast to the case of hard-core system. This is the typical result for our soft potential system.

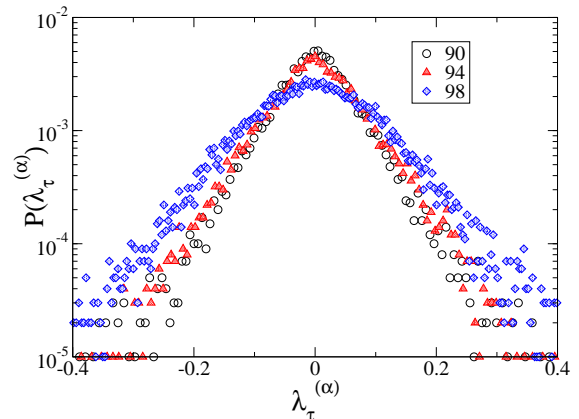


FIG. 4: Distribution of the finite time Lyapunov exponent $\lambda_\tau^{(\alpha)}$ where τ is equal to the period of re-orthonormalization and the index of LEs α is equal to 90, 94 and 98 respectively. The strong fluctuations of $\lambda_\tau^{(\alpha)}$ are one of the possible reasons for the disappearance of the step-wise structures in the Lyapunov spectrum. The parameter setting used here is: $N = 100$, $L = 1000$ and $T = 0.2$.

rule [27, 28]. From the enlargement shown in the inset of Fig. 3 for the part near $\lambda^{(\alpha)} \approx 0$, one can not see any step-wise structure in the Lyapunov spectrum in contrast to the case of hard-core systems [10]. This is the typical result obtained for our soft potential system.

The fluctuations in local instabilities is demonstrated by the distribution of finite-time LEs. In Fig. 4 such distributions for some LEs in the regime $\lambda \approx 0$ are presented. Fluctuations of the finite time Lyapunov exponents are quite large compared with the

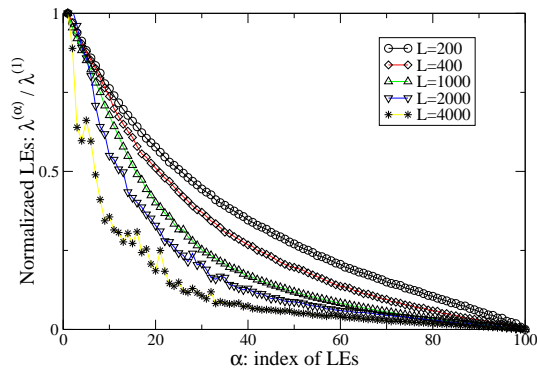


FIG. 5: Normalized Lyapunov exponents $\lambda^{(\alpha)}/\lambda^{(1)}$ with $L = 200, 400, 1000, 2000,$ and 4000 respectively. The Lyapunov spectrum becomes more and more bended as the particle density $\rho = N/L$ is decreased. This implies the separation of two time scales. Here $N = 100$ and $T = 0.2$.

difference between their mean values, i.e., $\sigma(\lambda_\tau^{(\alpha)}) \equiv \sqrt{\langle \lambda_\tau^{(\alpha)^2} \rangle - \langle \lambda_\tau^{(\alpha)} \rangle^2} \gg |\lambda^{(\alpha)} - \lambda^{(\alpha+1)}|$. Here $\langle \dots \rangle$ means time average. The strong fluctuations in local instabilities is one of the possible reasons for the disappearance of the step-wise structures in the Lyapunov spectra. It could also cause the mixing of nearby Lyapunov vectors. The mixing may be at the origin of the intermittency observed in the time evolution of the spatial Fourier transform of LVs (see Sect. III E).

D. Bending of Lyapunov spectrum with decreasing particle density

We studied also the influence of the particle density on the Lyapunov spectrum by increasing the length of the system with the particle number N kept fixed. As can be seen in Fig.5, the Lyapunov spectrum becomes more and more bended with increasing L . For the case of $L = 4000$, the spectrum can already be unambiguously divided into two regimes: In the upper regime, Lyapunov exponents decrease more quickly with increasing index than in the lower regime. This bending of the Lyapunov spectrum was related to the separation of two time scales in dilute particle systems [29]. We propose that one is the time of local collision events, and the other is due to the collective motion of the particles. For a system with high density, the collisions are so frequent that there are strong correlation between consecutive collisions and one can no longer separate them from each other. The collisions themselves contribute to the collective motion of the system. Therefore no time scale separation happens here and the LEs decrease gradually.

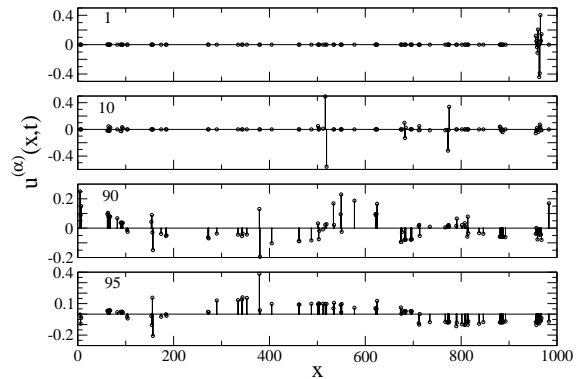


FIG. 6: $u^{(\alpha)}(x, t)$ for LVs with index $\alpha = 1, 10, 90,$ and 95 respectively. Notice that the former two are more localized while the latter two are more distributed. The parameter setting used here is: $N = 100, L = 1000$ and $T = 0.2$.

E. Spatial structure of LVs with $\lambda^{(\alpha)} \approx 0$

1. Coordinate fluctuation density (CFD)

Another quantity used to characterize the local instability of trajectories are Lyapunov vectors $\delta\Gamma^{(\alpha)}$, which represent expanding or contracting directions in tangent space. In the study of hard-core systems, Posch et al. found that coordinate part of the Lyapunov vectors corresponding to $\lambda \approx 0$ are of regular wave-like character [8, 9, 10]. They are referred to as *hydrodynamic Lyapunov modes*. We are searching here for the counterpart of these modes in our soft-potential system.

Remember that each of the LVs is consist of two parts: the displacement δx_i in coordinate space and δv_i in momentum space. In past studies of hydrodynamic Lyapunov modes in hard-core systems, only the coordinate part δx_i was considered. This is due to an interesting feature of LVs found in Ref.[12] which says that the angles between the coordinate part and the momentum part are always small, i.e, the two vectors are nearly parallel. Therefore, it is already sufficient to use only δx_i for studying $\delta\Gamma$. For our soft potential system, we find that the angles between the coordinate part and the momentum part are no longer as small as in the hard-core systems. However, we will still follow the tradition to study the coordinate part of LV first and come to the momentum part afterwards.

Analogous to the definition of microscopic densities in hydrodynamics [24], we define a quantity called *coordinate fluctuation density*

$$u^{(\alpha)}(x, t) = \sum_{i=1}^N \delta x_i^{(\alpha)} \cdot \delta(x - x_i). \quad (3)$$

Profiles of $u^{(\alpha)}(x, t)$ for some typical LVs of the Lennard-Jones system are presented in Fig. 6. It can be seen that $u^{(\alpha)}(x, t)$ for LVs corresponding to the largest Lyapunov exponents are highly localized, for example

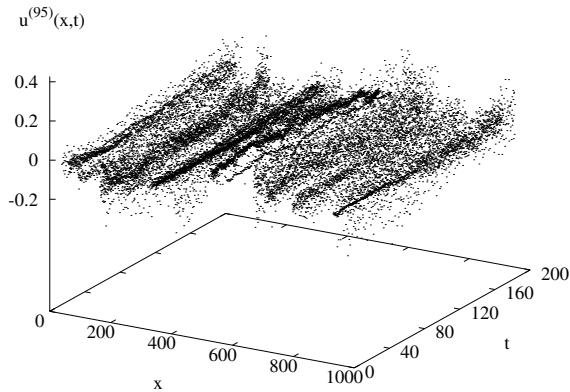


FIG. 7: Time evolution of $u^{(95)}(x, t)$. No clear wave structure can be detected. The parameter setting used here is: $N = 100$, $L = 1000$ and $T = 0.2$.

$u^{(1)}(x, t)$ and $u^{(10)}(x, t)$, while those for LV_{90} and LV_{95} are more distributed. The study on the localization of LV_1 is of long history [9, 10, 29, 30, 31, 32, 33, 34] and it was related to defect events in simulations of Benard convection [33]. We leave the discussion on this point to Sec.III F. The temporal evolution of $u^{(95)}(x, t)$ is shown in Fig. 7 in order to make the possibly existing wave-like structure more evident. A wave structure however, cannot unambiguously be detected here with the naked eye.

2. Spatial power spectrum of CFD and intermittency in its time evolution

Now we turn to the spatial Fourier transform of $u^{(\alpha)}(x, t)$, which reads

$$\begin{aligned} \tilde{u}_k^{(\alpha)}(t) &= \int u^{(\alpha)}(x, t) \exp(-ikx) dx \\ &= \sum_{j=1}^N \delta x_j^{(\alpha)} \cdot \exp[-ik \cdot x_j(t)] \end{aligned} \quad (4)$$

In previous studies, in order to make the wave structure more obvious, certain smoothing procedures in time or space were applied to the Lyapunov vectors. For a 1d hard-core system with only a few particles, this procedure has been shown to be quite useful in identifying the existence of hydrodynamic Lyapunov modes [15]. The success of this strategy relies on the fact that some of the Hydrodynamic Lyapunov modes (transverse modes) of hard-core systems are stationary [8]. Therefore, time averaging can indeed suppress the noise component and make the long wave-length modes more significant. For a soft potential system, all the Lyapunov vectors are not stationary due to the random mixing among them. Especially, for our one dimensional system studied here, no

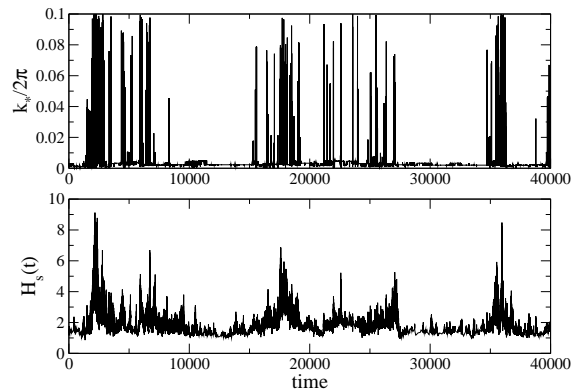


FIG. 8: Intermittent behavior of the peak wave-number k_* and spectral entropy $H_s(t)$ for the spatial Fourier spectrum of $u^{(95)}(x, t)$. The parameter setting used here is: $N = 100$, $L = 1000$ and $T = 0.2$.

transverse modes but only longitudinal Lyapunov modes exist. In consequence of this, the smoothing procedure is no longer very helpful for detecting the hidden regular modes and can even damages them [16]. Here we apply the spatial Fourier transformation to the instantaneous quantity $u^{(\alpha)}(x, t)$ instead. The algorithm offered especially for unevenly distributed data is very suitable for our case [35]. Furthermore, we take the long time average (and ensemble average) of the spatial Fourier spectrum

$$s_{uu}^{(\alpha)}(k, t) \equiv |\tilde{u}_k^{(\alpha)}(t)|^2 \quad (5)$$

since it is expected that in $S_{uu}^{(\alpha)}(k) \equiv \langle s_{uu}^{(\alpha)}(k, t) \rangle$ the contribution of stochastic fluctuations will be averaged out while the information about the collective modes will be left and accumulated. The following results show that this technique is quite successful in detecting the hidden collective modes.

The time evolution of the spatial Fourier spectrum $s_{uu}^{(95)}(k, t)$ for Lyapunov vector No. 95 is investigated in Fig. 8 as an example. Two quantities are recorded with time going on. One is the peak wave-number k_* , which marks the position of the highest peak in the spectrum $s_{uu}^{(\alpha)}(k, t)$ (see Fig. 9). The other is the spectral entropy $H_s(t)$ [36], which measures the distribution property of the spectrum $s_{uu}^{(\alpha)}(k, t)$. It is defined as:

$$H_s(t) = - \sum_{k_i} s_{uu}^{(\alpha)}(k_i, t) \ln s_{uu}^{(\alpha)}(k_i, t) \quad (6)$$

A smaller value of $H_s(t)$ means that the spectrum $s_{uu}^{(\alpha)}(k, t)$ is highly concentrated on a few values of k , i.e., these components dominate the behavior of the LV. Both of these quantities behave intermittently as shown in Fig. 8. Large intervals of nearly constant low values (*off state*) are interrupted by short period of bursts (*on state*) where they experience large values. Details of typical *on* and *off* states are shown in Fig. 9. It can be seen that the off state is dominated by the low wave-number

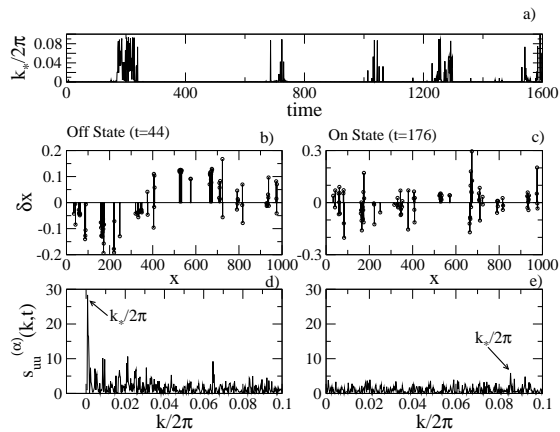


FIG. 9: a) Variation of the peak wave number k_* with time. b),c) Two typical snapshots of LV_{95} , *off* and *on* state at $t = 44$ and 176 respectively. d),e) their spatial Fourier transform. The spectrum for the off state has a sharp peak at small k_* while that for the on state has no dominant peak. The parameter setting used here is: $N = 100$, $L = 1000$ and $T = 0.2$.

components (see the sharp peak at low wave-number k_*) while the on state is more noisy and there are no significant dominant components. This intermittency in the time evolution of the spatial Fourier spectrum of LVs is a typical feature of soft potential systems. It is conjectured that this is a consequence of the mixing of nearby LVs caused by the wild fluctuations of local instabilities. One time scale can be extracted from the intermittency, i.e., the mean duration τ_{off} of the *off* state. We conjectured that this time scale is related to the life time of hydrodynamics Lyapunov modes. If the *off* state was viewed as a pure mode, the time τ_{off} is just the average life-time of such modes. Due to the mutual interaction among modes, the hydrodynamics Lyapunov modes in the soft potential systems are only of finite life-time. Further numerical work is needed in this direction to get more direct evidence.

In Fig.10, the time averaged spectral entropy $\langle H_s(t) \rangle$ is plotted against the index of the LVs. It increases gradually as the index decreases from $N - 2$. This means that LVs corresponding to smaller positive LEs are more localized in Fourier space, i.e., they have more wave-like character than those corresponding to larger LEs.

3. Dispersion relation of hydrodynamical Lyapunov modes

Now we consider the time averaged spatial Fourier spectrum $S_{uu}^{(\alpha)}(k)$ of LVs. Two cases with $L = 1000$ and 2000 are shown in Fig.11. It is not hard to recognize the sharp peak at $\lambda \approx 0$ in the contour plot of the spectrum. In increasing the Lyapunov exponents, the peak shifts to the larger wave number side. A dashed line is plotted to guide eyes how the wave number of the peak k_{max} changes with $\lambda^{(\alpha)}$. To further demonstrate this point,

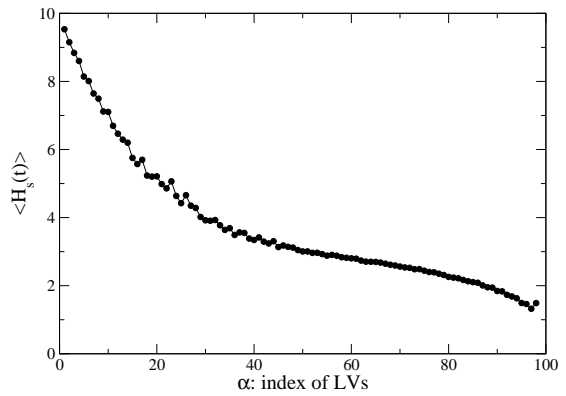


FIG. 10: Time-averaged spectral entropy $\langle H_s(t) \rangle$ vs. index of LVs. The gradual decrease of $\langle H_s(t) \rangle$ from $\alpha \approx 0$ means that LVs corresponding to smaller positive LEs are more localized in Fourier space, i.e. they have more wave-like character those that corresponding to larger LEs. The parameter setting used here is: $N = 100$, $L = 1000$ and $T = 0.2$.

in Fig.12, the value of the Lyapunov exponent $\lambda^{(\alpha)}$ is plotted versus k_{max} of corresponding LVs. We call this the *dispersion relation* of the hydrodynamical Lyapunov modes. The numerical fitting of the data shows that for $\lambda \approx 0$, $\lambda^{(\alpha)} \sim k_{max}^\gamma$ with the exponent $\gamma \approx 1.2$. However, a linear dispersion with quadratic corrections can not be excluded.

In order to show that the peak in $S_{uu}^{(\alpha)}(k)$ is not a result of the highly regular packing of particles in the broken-chain state, the static structure function [24]

$$S(k) \equiv \int G(r) \exp(-ikr) dr \quad (7)$$

for the case $L = 2000$ is plotted in the same figure as $S_{uu}^{(\alpha)}(k)$, where $G(r)$ is the pair correlation function shown in Fig. 2. It can be seen that $S(k)$ is nearly constant in the regime $k \approx 0$, the place where a sharp peak was observed in $S_{uu}^{(\alpha)}(k)$. The regular packing of particles causes the formation of a peak at $k/2\pi \approx 0.9$ in $S(k)$. This corresponds to a tiny peak at the same k -value in $S_{uu}^{(\alpha)}(k)$ for those LVs with $\lambda \approx 0$. These facts show clearly that the collective modes observed in LVs are not due to the regular packing of particles.

To further demonstrate the properties of these modes, in Fig.13, k_{max} is plotted versus index of LVs. As can be seen, for LVs with $\lambda \approx 0$, i.e. with $\alpha \approx N$, the value of k_{max} is quite small (see the enlargement in Fig. 14). For example, for $\alpha = 96, 97$, and 98 , $k_{max} = 2\pi/L$, which is the smallest wave number allowed by the periodic boundary conditions used. Another point to be noticed is the step structure in plotting k_{max} as function of α . This is similar to the degeneration of wave-numbers found in the hard-core case, although the steps here are not so regular. In the middle panel of Fig.13, the height $S_{uu}^{(\alpha)}(k_{max})$ of the highest peak in the time averaged spatial spectrum is plotted with index of LVs. Except LV No.99 and No.100

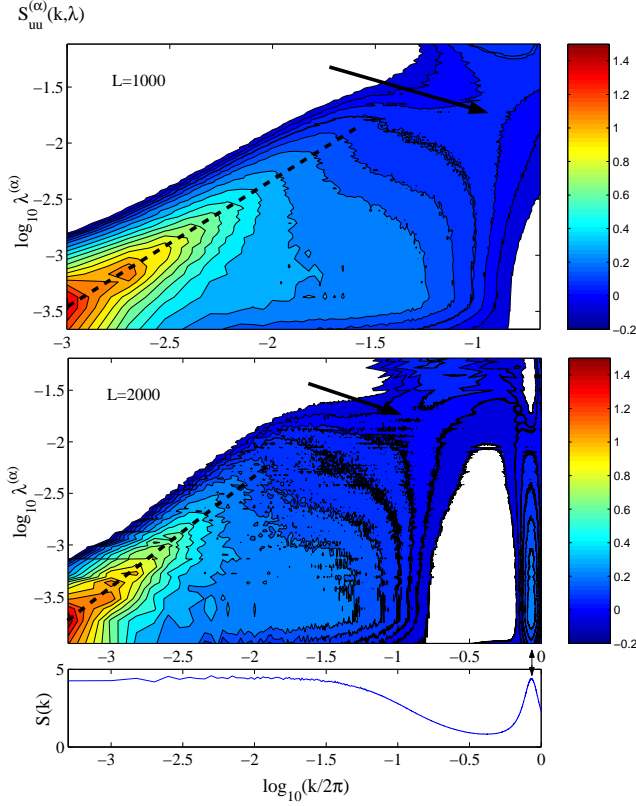


FIG. 11: (Color online) Contour plot of the spectrum $S_{uu}^{(\alpha)}(k)$ for $L = 1000$ and 2000 . There is a sharp peak at $k \approx 0$ and $\lambda \approx 0$. To guide eyes, a dashed line is plotted to show how the peak wave-number k_{max} changes with the variation of λ . The sudden jump in k_{max} is marked with an arrow. In total 58 samples for the case of $L = 1000$ (10 for $L = 2000$) are used averaging each for a period of $4 \times 10^6 h$. Here $T = 0.2$ and $N = 100$.

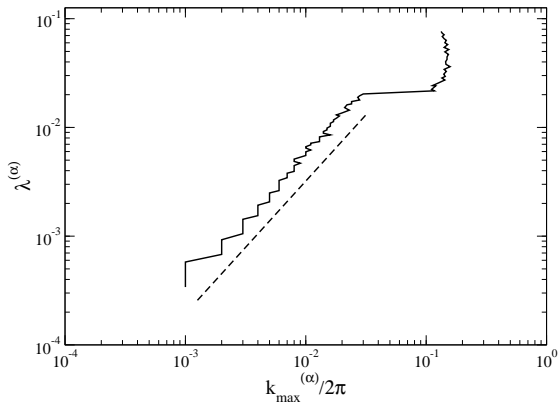


FIG. 12: The Lyapunov exponent $\lambda^{(\alpha)}$ is plotted as function of the wave-number k_{max} of the highest peak in the time averaged spatial Fourier spectrum of LVs. The dashed line is of the form $\lambda^{(\alpha)} \sim k_{max}^{1.2}$. The parameter setting used here is: $N = 100$, $L = 1000$ and $T = 0.2$.

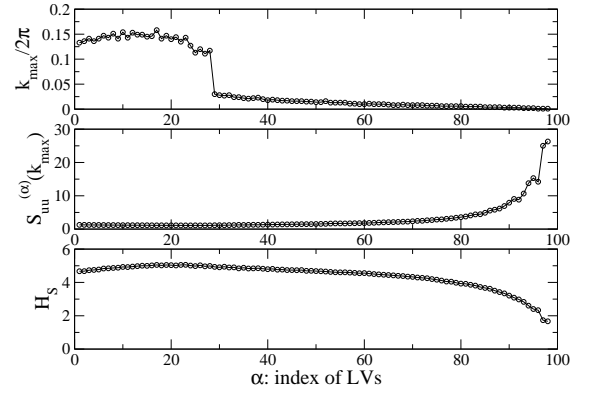


FIG. 13: (Upper panel) The wave-number k_{max} of the highest peak in the time averaged spatial Fourier spectrum of LVs. (Middle panel) The height $S_{uu}^{(\alpha)}(k_{max})$ of the highest peak in the time averaged spectrum. (Lower panel) The spectral entropy H_S for the averaged spectrum $S_{uu}^{(\alpha)}(k)$. The sudden jump in k_{max} implies the separation of time scales. The parameter setting used here is: $N = 100$, $L = 1000$ and $T = 0.2$.

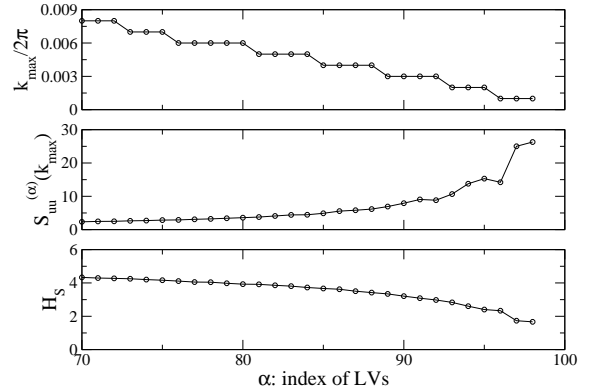


FIG. 14: Enlargement of Fig.13 for the part in the regime $\alpha \simeq N$.

for the conserved quantities, $S_{uu}^{(\alpha)}(k_{max})$ decreases gradually in decreasing the index from $N - 2$. Similar to the definition of the spectral entropy for the instantaneous spectrum $s_{uu}^{(\alpha)}(k, t)$ in Eq.6, one can also define a spectral entropy H_S for the averaged spectrum $S_{uu}^{(\alpha)}(k)$. The spectral entropy H_S for $S_{uu}^{(\alpha)}(k)$ is presented in the lower panel of Fig.13. It possesses a minimum at $\alpha = 98$ where the Lyapunov exponent is the smallest positive one. According to the definition of the spectral entropy, the minimum means that the spectrum of LV No.98 is most significantly dominated by a few components.

All of our results shown above give strong evidence that the Lyapunov vectors corresponding to the smallest positive LEs in our 1d Lennard-Jones system are highly dominated by a few components with small wave numbers, i.e, they are similar to the Hydrodynamic Lyapunov modes found in hard-core systems. The wave-like character becomes weaker and weaker as the value of LE is increased gradually from zero.

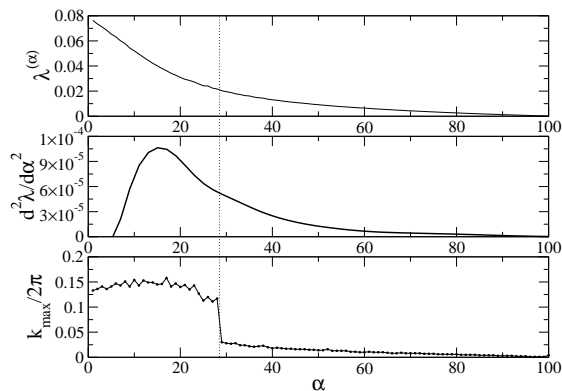


FIG. 15: The Lyapunov spectrum $\lambda^{(\alpha)}$ (upper panel), $d^2\lambda/d\alpha^2$ (middle panel) and k_{max} vs. the index α . The parameter setting used here is: $N = 100$, $L = 1000$ and $T = 0.2$.

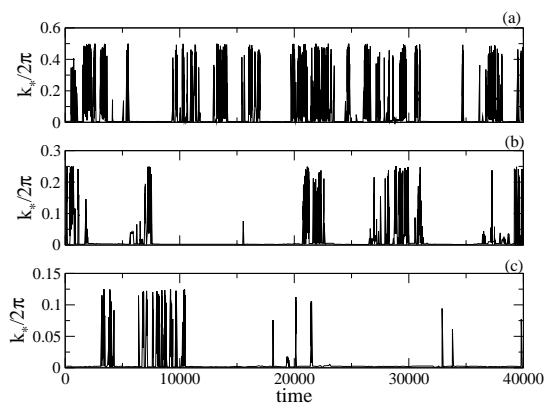


FIG. 16: Same as top panel of Fig. 8, but with different density (a) $\rho = 1/2$, (b) $1/4$ and (c) $1/8$ respectively. Here $T = 0.2$ and the particle number $N = 100$.

4. Separation of time scales

Another interesting point in Fig.13 is the sudden jump in k_{max} at $\alpha \approx 26$ which divides the whole set of LVs into two groups. It is believed that this sudden jump is related with the bending of the LE spectrum and the separation of time scales in a dilute system. As shown in Fig. 15, the sudden jump is in the regime where the LEs spectrum is most strongly bended, although it is not at the exact place where $d^2\lambda^{(\alpha)}/d\alpha^2$ experiences the maximal value. Further work is needed to reveal the underlying connection between these phenomena.

5. Influence of density and temperature

To study how the change in density influences the behavior of LVs, we increase the length L of the system from 200 to 4000 with the particle number N kept fixed at 100. From the time evolution of k_* shown in Fig.16, one sees that, in increasing the density $\rho = N/L$, the occurrence of the *on*-state becomes more frequent, i.e.,

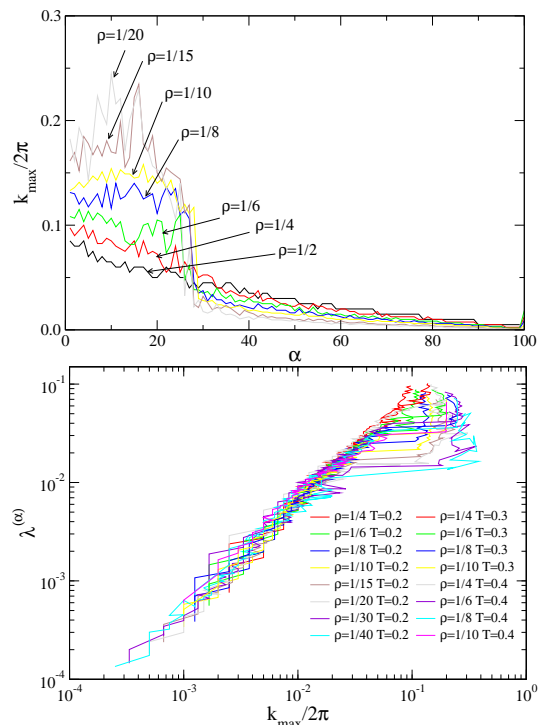


FIG. 17: (Color online) (upper panel) The wave-number k_{max} of the highest peak in the time-averaged spatial Fourier spectrum of LVs as function of LV index α . (lower panel) the Lyapunov exponent $\lambda^{(\alpha)}$ as function of k_{max} . Note that in the lower panel, all data from simulations with different densities and temperatures collapse to a single curve. Fitting of the low wave-number part to a power-law function $\lambda^\alpha \sim k_{max}^\gamma$ gives $\gamma \approx 1.2 \pm 0.1$. Here $N = 100$ and $T = 0.2$.

the domination of low wave-number components is much weaker. The spatial Fourier spectrum for LVs with LEs in the regime $\lambda^{(\alpha)} \simeq 0$, however, are always dominated by certain low wave-number components irrespective of the density (see Fig.17).

An important point is the collapse of data of dispersion relations from simulations with various densities and temperatures to a single curve (see lower panel of Fig.17). This means, for hydrodynamic Lyapunov modes in our system, there is a universal dispersion function $\lambda_\alpha(k)$ irrespective to the particle density and the system temperature. Fitting of the data to a power-law function $\lambda_\alpha \sim k_{max}^\gamma$ says the value of the exponent γ is 1.2 ± 0.1 although a linear dispersion with quadratic corrections cannot be excluded.

Another feature of Fig.17 (upper panel) is that the sudden jump in k_{max} disappears as the system density N/L is increased. This is consistent with our above discussion that the separation of time scales is only significant in dilute systems.

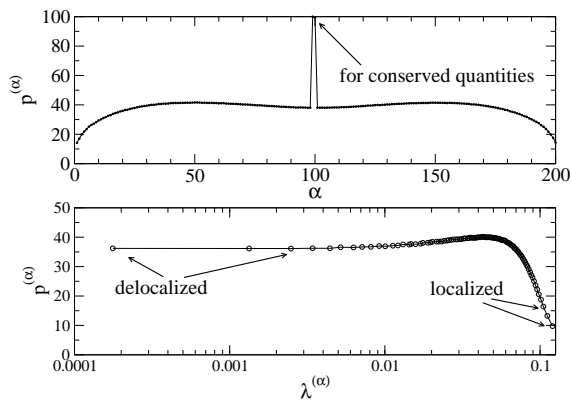


FIG. 18: Time-averaged participation number $p^{(\alpha)}$ vs. index of LVs (upper panel) and $\lambda^{(\alpha)}$ (lower panel). The parameter setting used here is: $N = 100$, $L = 110$ and $T = 1.6$.

6. Dynamics of the momentum part

Now we turn to investigations on the spatial Fourier spectrum of the momentum part of LVs. Unfortunately, all the spectra are more or less homogeneously distributed on all wave-numbers. For all the cases checked, no wave-like structure can be identified as for the coordinate part. One may wonder why no mode-like collective motion is observed in the momentum part. There are two possibilities, one is that the momentum part does contain information similar to the coordinate part but it is too weak to be detected here due to the strong noise. The other is that there is no similarity between the two parts at all and regular long wave-length modes exist only in the coordinate part. Further work is needed to clarify which one is correct.

F. Localization properties of LVs

To study the localization of LVs, we employ the participation number, which is defined as:

$$p \equiv \left[\sum_{i=1}^N (\delta x_i^2 + \delta v_i^2)^2 \right]^{-1} \quad (8)$$

for a Lyapunov vector $(\delta x_i^{(\alpha)}, \delta v_i^{(\alpha)})$ [37]. This is a standard quantity used in the study of disorder-induced localization [38], which roughly measures the number of particles which contribute to the Lyapunov vector. For the homogeneous Lyapunov vector LV_N with $w^2 \equiv \delta x_i^2 + \delta v_i^2 = 1/N$, which corresponds to one of the zero-value LEs, p gets its maximal value N . In decreasing the index of LVs, LEs become larger and larger. Accompanying to this, the participation number $p^{(\alpha)}$ decreases as presented in Fig. 18, where the variation of the time-averaged value of $p^{(\alpha)}$ versus index α and $\lambda^{(\alpha)}$ are plotted. The decrease of $p^{(\alpha)}$ implies that LVs become more and more localized with decreasing α .

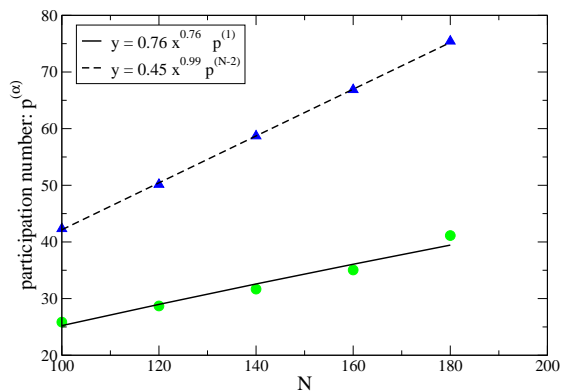


FIG. 19: Time-averaged participation number $p^{(1)}$ and $p^{(N-2)}$ vs. particle number N . The parameter setting used here is: $L/N = 1.1$ and $T = 1.6$.

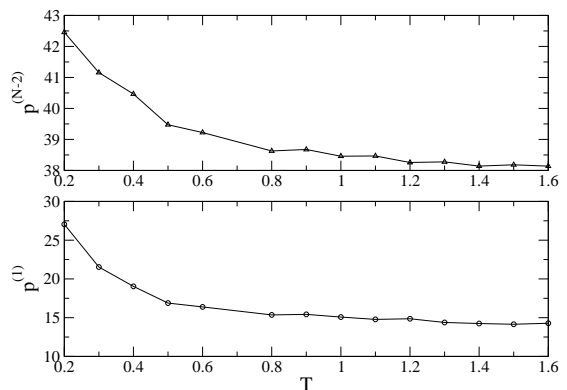


FIG. 20: a) Time-averaged participation number $p^{(1)}$ and $p^{(N-2)}$ vs. temperature T . The parameter setting used here is: $N = 200$ and $L = 220$.

One should note that $p^{(N-2)}$ for LV_{N-2} corresponding to the smallest positive Lyapunov exponent is significantly different from $p^{(N)} = N$ for LV_N with $\lambda^{(N)} = 0$. In Fig. 18, $p^{(N-2)} \approx 40$ while $p^{(N)} = 100$. In the study of space-time chaos, a commonly used measure for quantifying spatio-temporal disorder is the fractal dimension D . A spatio-temporal chaotic system is generally extensive, with the fractal dimension D in proportion to its volume V . According to this, a bounded intensive quantity named dimension correlation length is defined $\xi_D = \lim_{V \rightarrow \infty} (D/V)^{-1/d}$. Based on the intuitive thought that a spatio-temporal chaotic system is composed of many subsystems and that these subsystem are uncorrelated if they are far apart, it is expected that ξ_D is proportional to the two-point correlation length, which measures the spatial disorder of the system. A particular fractal dimension, the Lyapunov dimension $D_{\mathcal{L}}$ can be easily obtained using the Kaplan-Yorke formalism which relates the Lyapunov dimension to Lyapunov exponents of the system [39]. For a Hamiltonian system like the one studied here, Lyapunov exponents are paired, i.e. $\lambda^{(\alpha)} + \lambda^{(2dN-\alpha)} = 0$ due to the symplectic structure

of the system [27, 28]. According to the Kaplan-Yorke formalism, the Lyapunov dimension for a d -dimensional Hamiltonian spatio-temporal chaotic will be $D_{\mathcal{L}} = 2dN$ in spite of the details of dynamics. Although $D_{\mathcal{L}}$ defined in such way is proportional to the volume of the system i.e., reflects the extensiveness of the system, its value is always a constant irrespective of the temperature change. However the two-point correlation length does change with the temperature and it even becomes divergent as a phase transition is encountered. In this sense, the Lyapunov dimension $D_{\mathcal{L}}$ and the dimension correlation length ξ_D are only trivially defined here and not good quantities to characterize spatio-temporal Hamiltonian chaos. Here we propose a new length scale based on the participation number of LVs:

$$\xi_p^{(\alpha)} \equiv \left(\frac{p^{(\alpha)}}{N} \cdot V \right)^{1/d} \quad (9)$$

where d is the dimension of the physical space and V is the system volume which is simply L for our $d = 1$ case here. According to the fact we mentioned above, $\xi_p^{(N-2)}$ for the smallest positive Lyapunov exponent is a nontrivial value depending on the state of the system.

Now we first check the extensiveness of $\xi_p^{(N-2)}$. The fit of the numerical data in Fig. 19 gives $p^{(N-2)} \sim N^{0.99}$. This tells us $p^{(N-2)}$ (and consequently $\xi_p^{(N-2)}$) is proportional to the system size N , i.e., it is an extensive quantity. The dependence of $p^{(1)}$ for the largest Lyapunov exponent on N is shown in the same plot. It is fitted with $p^{(1)} \sim N^{0.76}$, i.e., the Lyapunov vector for the largest LE is highly localized in space [10, 29, 32]. This is consistent with our above observation (see Fig. 6).

Then we study the temperature dependence of this newly defined length scale. For a 200-particle system, the temperature is increased from 0.4 to 1.6. Results of the simulation are shown in Fig. 20, where the variation of $p^{(1)}$ with temperature T is also presented. From the plot, one can see that $p^{(N-2)}$ (and consequently $\xi_p^{(N-2)}$) decreases gradually with the increase in temperature. This agrees with the intuitive expectation that, increasing of the temperature makes the fluctuation in the system stronger and stronger and renders the system becoming more and more disordered.

IV. CONCLUSION AND DISCUSSION

In this paper, we presented numerical results about the Lyapunov instability of a Lennard-Jones system. Our simulations show that the step-wise structure found in the Lyapunov spectrum of hard-core systems disappears completely here. This is conjectured due to the strong fluctuations in the finite-time LEs [10]. A new technique [40] based on a spatial spectral analysis is employed to reveal the hidden long wave-length structure in LVs. A significantly sharp peak with low wave-number is found in the resultant spatial Fourier spectrum for LVs with

$\lambda \simeq 0$. This serves as strong evidence that hydrodynamic Lyapunov modes do exist in the soft-potential systems [41]. Another important finding is that the dispersion relation for hydrodynamic Lyapunov modes, $\lambda^{(\alpha)}$ versus k_{max} , appears to be universal irrespective of system temperature and particle density.

In the study of two-dimensional and quasi-one-dimensional hard-core systems, two kinds of hydrodynamic Lyapunov modes are identified [10, 15]. One is referred to as transverse and the other is called longitudinal. The former modes do not propagate while the latter can [10]. According to this classification, for the transverse Lyapunov modes, taking the time average can be an useful way to identify the wave-like structure. In contrast to this, the detection of the longitudinal Lyapunov modes is a relatively difficult task since due to its propagation time-averaging is no longer a suitable method to suppress the fluctuations [15]. For the case of soft potential system, strong fluctuations in local instabilities leads to the occasional mixing among Lyapunov vectors. This is partially reflected in the intermittent time evolution of spatial Fourier spectrum of LVs. Therefore the hydrodynamic Lyapunov modes in a soft-potential system are more vague and more difficult to observe [16].

In the study of the hard-core case, it is conjectured that degeneracies in the Lyapunov spectrum and in wavenumbers of hydrodynamic Lyapunov modes are determined by the intrinsic symmetries of the Hamiltonian and the boundary conditions. There is no contradiction between this statement and the results reported here. The crucial point is the life-time of hydrodynamic Lyapunov modes. The above statement is for the ideal case of pure modes with infinite long life-time. For the Lennard-Jones system studied here, strong fluctuation in local instability leads to the mutual interaction and mixing among modes, which renders the life-time of modes becoming finite. On the other hand, Lyapunov exponents are global quantities of the system, which are the result of a time-average along a long trajectory wandering all over the phase space allowed. Due to the mixing among modes, they no longer correspond to certain pure modes but to a mixture of several modes. Therefore the degeneration predicted on the basis of a symmetry analysis can not be seen here. Actually, fluctuations in local instabilities do exist in all dynamical systems. However, for the hard-core systems, it is relatively weak in the regime of $\lambda \approx 0$ (see Fig.12 in [10] for the comparison of fluctuations in local instabilities for the two cases). There the mixing among modes is quite rare and weak. The life-times of the modes with $\lambda \approx 0$ are so long that one can not feel it during the finite simulation time. Evidence for our argument above comes from the fact that as the fluctuations in local instabilities of hard-core system become stronger and stronger in increasing LEs from $\lambda \approx 0$, the degeneration in LEs becomes worse and worse, i.e. the steps become steeper and steeper (see Fig.12 and Fig. 8 in Ref.[10]). In this work, Fourier spectral analysis has been shown to be quite successful in detecting the hidden

wave-like structures in LVs. A more general theoretical consideration of this method will be given elsewhere [40].

Until now, only the coordinate part of the LVs are used in the study of hydrodynamic Lyapunov modes. For the case of hard-core system, this is reasonable due to the interesting feature of LVs found in [12] that the angles between the coordinate part and the momentum part are always small, i.e, the two vectors are nearly parallel. For our soft potential system, we find that the angles between the coordinate part and the momentum part are no longer as small as in the hard-core systems. Even for the hard-core system, recent results show that the two vectors are not always parallel [29]. Therefore it is necessary to reconsider the momentum part of LVs. Due to the specific feature of Hamiltonian systems, the momentum part of a LV with $\lambda > 0$ is identical to the coordinate part of a LV with $-\lambda$. This ensures that the study of only the coordinate part of LVs is sufficient. But now one need to deal with LVs corresponding to both positive and negative LEs. In general, the behavior of LVs with negative LEs should be different from those with positive ones. For the case reported in the current paper, there is no wave-like structure being observed in the former.

We studied also the influence of density and temperature changes on the features of LVs and LEs. One effect of decreasing the density is that the Lyapunov spectrum becomes more and more bended. The relation of

the bending in the Lyapunov spectrum with the separation of time scales was discussed recently in the work of Taniguchi and Morriss [29]. It is obvious that, the collisions between particles become more and more rare as the density is decreased. They turn to be highly localized events since they happen at only a few places at one moment. Therefore, the time scale of local collision events, which is related to the largest LEs [2], is well separated from that for the collective motion of the system, corresponding to the near-zero LEs. A further point is the sudden jump found in k_{max} of the time-averaged spatial Fourier spectrum of LVs. It divides the whole set of LVs into two groups. The place of this sudden jump is in the regime where the Lyapunov spectrum is strongly bended. Further work is needed to reveal the underlying connection between these phenomena.

Acknowledgments

We thank H. A. Posch, W. Kob, A. S. Pikovsky, W. Just and A. Latz for fruitful discussions and W. Kob in addition for providing us with his MD simulation code, on which our program is built. Financial support from SFB393 within the project "Long time behavior of large dynamical systems" is gratefully acknowledged.

-
- [1] J.-P. Eckmann, D. Ruelle, *Rev. Mod. Phys.* **57**, 617 (1985); E. Ott, *Chaos in Dynamical Systems* (Cambridge University Press, Cambridge 1993).
- [2] N.S. Krylov, *Works on the Foundations of Statistical Mechanics* (Princeton University Press, Princeton, 1979).
- [3] P. Gaspard, *Chaos, Scattering, and Statistical Mechanics* (Cambridge University Press, Cambridge, 1998).
- [4] J.P. Dorfman, *An Introduction to Chaos in Nonequilibrium Statistical Mechanics* (Cambridge University Press, Cambridge, 1999).
- [5] D.J. Evans, G.P. Morriss, *Statistical Mechanics of Nonequilibrium Liquids* (Academic, New York, 1990).
- [6] Wm.G. Hoover, *Computational Statistical Mechanics* (Elsevier, New York, 1991).
- [7] Wm.G. Hoover, *Time Reversibility, Computer Simulation, and Chaos* (World Scientific, Singapore, 1999).
- [8] Lj.Milanović, H.A. Posch, and Wm.G. Hoover, *Molec. Phys.* **95**, 281 (1998), H.A. Posch and R. Hirschl, in *Hard ball systems and the Lorentz gas*, p.269, EMS Vol. 101, Ed. D. Szasz (Springer, Berlin, 2000).
- [9] H.A. Posch, Ch. Forster, in *Collective Dynamics of Nonlinear and Disordered Systems*, p.309, Eds. G. Radons, W. Just, and P. Häussler (Springer, Berlin, 2004), in print.
- [10] C. Forster, R. Hirschl, H.A. Posch and Wm.G. Hoover, *Physics D* **187**, 294 (2004).
- [11] J.-P. Eckmann and O. Gat, *J. Stat. Phys* **98**, 775 (2000).
- [12] S. McNamara and M. Mareschal, *Phys. Rev. E* **64**, 051103 (2001); M. Mareschal and S. McNamara, *Physics D* **187**, 311 (2004).
- [13] A. de Wijn and H. van Beijeren, *nlin.CD/0312051*.
- [14] T. Taniguchi and G.P. Morriss, *Phys. Rev. E* **65**, 056202 (2002).
- [15] T. Taniguchi and G.P. Morriss, *Phys. Rev. E* **68**, 026218 (2003).
- [16] Wm.G. Hoover, H.A. Posch, C. Forster, C. Dellago and M. Zhou, *J. Stat. Phys.* **109**, 765 (2002).
- [17] M.C. Cross and P.C. Hohenberg, *Rev. Mod. Phys.* **65** 851 (1993).
- [18] W. Kob and H.C. Andersen, *Phys. Rev. E* **51**, 4626 (1995).
- [19] G. Benettin, L. Galgani and J. M. Strelcyn, *Phys. Rev. A* **14**, 2338 (1976).
- [20] I. Shimada and T. Nagashima, *Prog. Theor. Phys.* **61**, 1605 (1979).
- [21] H. A. Posch and W. G. Hoover, *Phys. Rev. A* **38**, 473 (1988).
- [22] A. Pikovsky, *Chaos* **3**, 225 (1993).
- [23] C. Dellago, W.G. Hoover and H.A. Posch, *Phys. Rev. E* **65**, 056216 (2002).
- [24] J.P. Boon and S. Yip, *Molecular Hydrodynamics* (McGraw-Hill, New York, 1980).
- [25] F.H. Stillinger, *Phys. Rev. E* **52**, 4685 (1995).
- [26] V.I. Oseledec, *Trans. Mosc. Math. Soc.* **19**, 197 (1968).
- [27] D.J. Evans, E.G.D. Cohen and G.P. Morriss, *Phys. Rev. A* **42**, 5990 (1990).
- [28] C.P. Dettmann and G.P. Morriss, *Phys. Rev. E* **53**, R5545 (1996).
- [29] T. Taniguchi and G.P. Morriss, *Phys. Rev. E* **68**, 46203 (2003).

- [30] Y. Pomeau, A. Pumir, and P. Pelce, *J. Stat. Phys.* **37**, 39 (1984); K. Kaneko, *Physica D* **23**, 436 (1986).
- [31] G. Giacomelli and A. Politi, *Europhys. Lett.* **15**, 387 (1991).
- [32] A. Pikovsky and A. Politi, *Nonlinearity* **11**, 1049 (1998); A. Pikovsky and A. Politi, *Phys. Rev. E* **63**, 036207 (2001).
- [33] W. Pesch, D.A. Egolf, I.V. Melnikov and R.E. Ecke, *Nature* **404**, 733 (2000).
- [34] Lj. Milanović, H.A. Posch, and Wm.G. Hoover, *Chaos* **8**, 455 (1998)
- [35] W.H. Hess, S.A. Teukolsky, W.T. Vetterling, and B.P. Flannery, *Numerical Recipes in Fortran 77* (Cambridge University Press, Cambridge, 1992), p.569.
- [36] R. Livi, M. Pettini, S. Ruffo, M. Sparpaglione and A. Vulpiani, *Phys. Rev. A* **31**, 1039 (1985).
- [37] Here we follow Ref. [32] to construct a scalar variable $\delta x_i^2 + \delta v_i^2$ to study the localization of LVs.
- [38] D.J. Thouless, *Phys. Rep.* **13c**, 93 (1974); F. Wegner, *Z. Phys. B* **36**, 209 (1979).
- [39] J. Kaplan and J. A. Yorke, *Springer Lecture Notes in Mathematics* **730**, p.204 (1979).
- [40] G. Radons and H. L. Yang, *Static and Dynamic Correlations in Many-Particle Lyapunov Vectors*, preprint.
- [41] After this work was finished, we heard from H. Posch that now these modes are also found in one- and two-dimensional fluids with Weeks-Chandler-Anderson (WCA) interaction potentials; H.A. Posch, talk given at DPG-Frühjahrstagung, Regensburg, 8-12 March 2004, Ch. Forster and H.A. Posch, in preparation.